

Mechanisms of Atomic Layer Deposition on Substrates with Ultrahigh Aspect Ratios

S. O. Kucheyev,* J. Biener, T. F. Baumann, Y. M. Wang, and A. V. Hamza

Nanoscale Synthesis and Characterization Laboratory, Lawrence Livermore National Laboratory, Livermore, California 94551

Z. Li, D. K. Lee, and R. G. Gordon

Department of Chemistry and Chemical Biology, Harvard University, Cambridge, Massachusetts 02138

Received June 22, 2007. In Final Form: October 23, 2007

Atomic layer deposition (ALD) appears to be uniquely suited for coating substrates with ultrahigh aspect ratios ($\geq 10^3$), including nanoporous solids. Here, we study the ALD of Cu and Cu_3N on the inner surfaces of low-density nanoporous silica aerogel monoliths. Results show that Cu depth profiles in nanoporous monoliths are limited not only by Knudsen diffusion of heavier precursor molecules into the pores, as currently believed, but also by other processes such as the interaction of precursor and reaction product molecules with pore walls. Similar behavior has also been observed for Fe, Ru, and Pt ALD on aerogels. On the basis of these results, we discuss design rules for ALD precursors specifically geared for coating nanoporous solids.

Technological applications of nanoporous solids, directly related to their large surface areas or low densities, are numerous.¹ However, mature synthesis technologies, with flexibility and control over material properties, have been developed for only a limited number of nanoporous systems, such as porous polymers, sol–gel-derived silica, alumina, and zeolites.¹ It is, therefore, highly attractive to develop a tool for uniform coating of the inner surfaces of the existing robust nanoporous systems with control over the elemental composition, thickness, and morphology of the coating.^{2–7} Unfortunately, the ultrahigh effective aspect ratios inherent to bulk nanoporous solids severely limit the usefulness of most deposition techniques, such as physical vapor deposition and non-self-limiting versions of chemical vapor deposition.⁸

These limitations have been overcome in several recent reports^{2–4} demonstrating atomic layer deposition (ALD), which is also known as atomic layer epitaxy and molecular layering⁸ as a very promising method for controlled coating of the inner surfaces of monolithic nanoporous aerogel (AG) substrates. Such AGs are sol–gel-derived open-cell nanoporous solids, typically with a large degree of mesoporosity ($\geq 80\%$) and high surface

area ($\geq 50 \text{ m}^2 \text{ g}^{-1}$).⁹ A closer analysis of the previous reports,^{2–7} however, reveals that the only successful depositions on the inner surfaces of nanoporous monoliths have been ALD coatings with Al_2O_3 ,² ZnO ,² and W ,^{3,4} with $\text{Al}(\text{CH}_3)_3$, $\text{Zn}(\text{C}_2\text{H}_5)_2$, and WF_6 as metal-containing precursors, respectively. All these precursors (and their reaction byproducts) were volatile enough so that the pressure in the deposition chamber was ~ 10 Torr. These depositions resulted in uniform coatings that penetrated hundreds of microns into the AGs. All our other attempts to uniformly coat the inner surfaces of AG monoliths with metals, including Ru,⁵ Pt,⁶ Fe,⁷ and Cu (the present work), have deposited metal into monoliths only up to a depth of tens of microns. The reason for the less deep penetration of the latter metals could be that the partial pressures of their precursors in the deposition zone did not exceed ~ 0.1 Torr, which is ~ 2 orders of magnitude less than the pressures of the more volatile precursors used in refs 2–4.

In this paper, we study the mechanisms and address current challenges of ALD on nanoporous monoliths with typical effective aspect ratios of $\geq 10^3$.¹⁰ In particular, we present details of ALD of Cu and Cu_3N onto low-density silica AGs. Using the Cu(I) *N,N'*-di-*sec*-butylacetamidinate $[\text{Cu}(\text{tBu-Me-amd})_2]$ precursor (Figure 1a), recently developed by Li et al.,¹¹ we studied the penetration of Cu and Cu_3N into nanoporous AGs. This study shows that the precursors and process parameters developed for successful ALD on substrates with moderate aspect ratios ($\leq 10^3$) could have limited suitability for coating bulk nanoporous solids. Much more volatile precursors will likely be needed for ALD on substrates with ultrahigh aspect ratios. We also demonstrate some limitations of the currently accepted picture that ALD on substrates with high aspect ratios is controlled mainly by Knudsen

* Corresponding author.

(1) See, for example, *Handbook of Porous Solids*; Schuth, F., Sing, K. S. W., Weitkamp, J., Eds.; Wiley-VCH: Weinheim, Germany, 2002.

(2) Kucheyev, S. O.; Biener, J.; Wang, Y. M.; Baumann, T. F.; Wu, K. J.; van Buuren, T.; Hamza, A. V.; Satcher, J. H., Jr.; Elam, J. W.; Pellin, M. J. *Appl. Phys. Lett.* **2005**, *86*, 083108.

(3) Baumann, T. F.; Biener, J.; Wang, Y. M.; Kucheyev, S. O.; Nelson, E. J.; Satcher, J. H., Jr.; Elam, J. W.; Pellin, M. J.; Hamza, A. V. *Chem. Mater.* **2006**, *18*, 6106.

(4) Elam, J. W.; Libera, J. A.; Pellin, M. J.; Zinovev, A. V.; Greene, J. P.; Nolen, J. *Appl. Phys. Lett.* **2006**, *89*, 053124.

(5) Biener, J.; Baumann, T. F.; Wang, Y. M.; Nelson, E. J.; Kucheyev, S. O.; Hamza, A. V.; Kemell, M.; Ritala, M.; Leskela, M. *Nanotechnology* **2007**, *18*, 055303.

(6) Giri, S.; Baumann, T. F.; Biener, J.; Kucheyev, S. O.; Bent, S. F.; Hamza, A. V. Unpublished work, 2006.

(7) Li, Z.; Gordon, R. G.; Kucheyev, S. O.; Baumann, T. F.; Biener, J.; Hamza, A. V. Unpublished work, 2007.

(8) See, for a example, a review by Puurunen, R. L. *J. Appl. Phys.* **2005**, *97*, 121301 and references therein.

(9) See, for example, reviews by Hüsing, N.; Schubert, U. *Angew. Chem., Int. Ed. Engl.* **1998**, *37*, 22 and Pierre, A. C.; Pajonk, G. M. *Chem. Rev.* **2002**, *102*, 4243.

(10) A 1-mm-thick AG monolith with an average pore diameter of 10 nm has a very high effective aspect ratio of 10^5 . Note that the recent studies of ALD on nanoporous monoliths^{2–7} were stimulated by numerous previous reports of uniform coatings of substrates with more moderate aspect ratios of $\leq 10^3$.⁸

(11) Li, Z.; Barry, S. T.; Gordon, R. G. *Inorg. Chem.* **2005**, *44*, 1728.

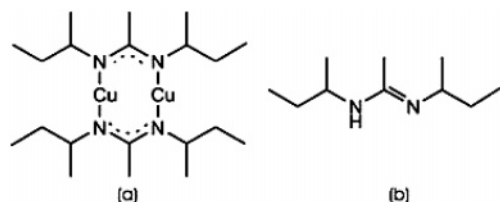


Figure 1. Molecular structure of the Cu(I) *N,N'*-di-*sec*-butylacetamidate [Cu(^{*t*}Bu-Me-amd)]₂ precursor (a) and the *N,N'*-di-*sec*-butylacetamidine reaction product (b).

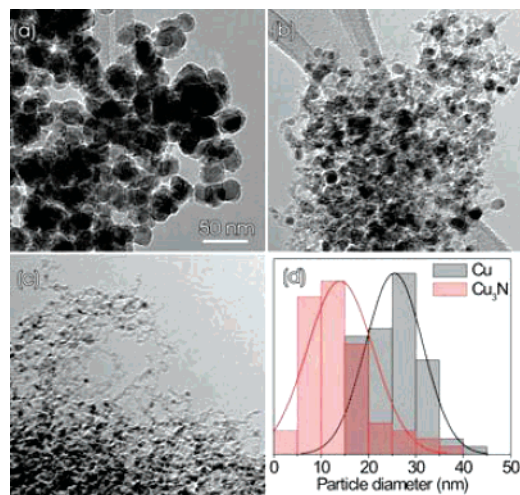


Figure 2. Bright-field transmission electron microscopy images of Cu (a) and Cu₃N (b) coated AGs with an initial density of 25 mg cm⁻³. ALD parameters: $t_{\text{CuAMD}} = t_{\text{H}_2/\text{NH}_3} = 150$ s, $t_{\text{pur1}} = t_{\text{pur2}} = 30$ s, $N_{\text{cyc}} = 50$. Uncoated AG is shown in panel c for comparison. All three images are of the same magnification. Normalized distributions of Cu and Cu₃N particle diameters are shown in panel d.

diffusion of precursor molecules.^{2-7,12,13} Instead, we speculate that the depth uniformity of coating is also influenced by surface interactions of precursor and reaction product molecules.

The morphology of Cu- and Cu₃N-coated as well as uncoated AGs is illustrated in Figure 2.¹⁴ Both Cu and Cu₃N coatings consist of crystalline nanoparticles, with relatively broad size distributions (Figure 2d), deposited on amorphous SiO₂ ligament surfaces. The average diameters of the Cu and Cu₃N nanoparticles shown in Figure 2 are 25 and 14 nm, respectively.¹⁵ Such a particulate morphology of coatings on AGs is not unexpected on the basis of previous studies of both Cu and Cu₃N depositions onto nominally flat substrates under similar ALD conditions.^{16,17} We also note that deposition at 190 °C results in a slightly nonstoichiometric nitride film (Cu₃N_{1-x});¹⁷ for brevity, we refer to such coatings as Cu₃N in this paper.

Representative Rutherford backscattering (RBS) spectra are illustrated in Figure 3,¹⁴ showing experimental data points and

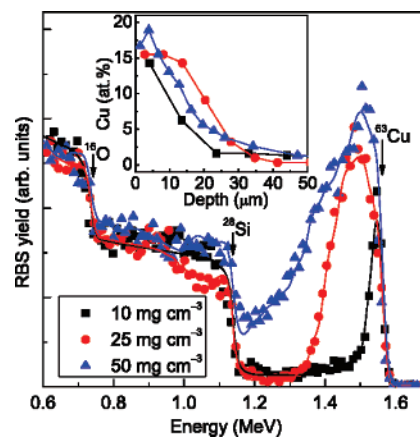


Figure 3. RBS spectra from Cu-coated AGs with different initial densities, as indicated. The positions of the surface peaks of O, Si, and Cu are denoted by arrows. For clarity, only every third experimental point is depicted. Solid lines are results of RUMP simulation. ALD parameters for all three AGs: $N_{\text{cyc}} = 10$, $t_{\text{CuAMD}} = t_{\text{H}_2/\text{NH}_3} = t_{\text{pur1}} = t_{\text{pur2}} = 1500$ s. The inset shows depth profiles of the Cu concentration extracted from these RBS spectra.

Table 1. Some Properties of Amorphous Silica AG Substrates Used in This Study

density (mg cm ⁻³)	porosity (%)	SA ^a (m ² g ⁻¹)	APD ^b (nm)
10	99.5	350	27
25	98.9	480	18
50	97.7	530	18

^aSA = BET surface area. ^bAPD = BJH average pore diameter.

simulation curves for three Cu-coated AGs with initial densities of 10, 25, and 50 mg cm⁻³. The inset in Figure 3 shows depth profiles of Cu extracted from such RBS spectra. It is seen from Figure 3 that the Cu concentration drops rapidly with increasing depth from the monolith surface for all three AGs. The Cu *penetration depth*, defined here as the depth at which the Cu concentration drops to 1/e of its maximum value, is < 25 μm and is very slightly affected by the initial density of AG monoliths. This is in contrast to what would be expected if deposition were limited only by Knudsen diffusion of Cu precursor molecules. Indeed, in this case, the deposition depth would have increased with decreasing initial density of AG monoliths since the average pore diameters and, hence, diffusion coefficients¹⁸ are generally larger for lower density AGs (see Table 1).

For a better understanding of the mechanisms controlling coating depth in AG monoliths, we have performed a systematic study for both Cu and Cu₃N ALD processes. Figures 4 and 5 summarize our results,¹⁴ showing the dependencies of the three major parameters—Cu thickness on SiO₂ wafers, the maximum Cu concentration in AGs,¹⁹ and Cu penetration depth—on the number of ALD cycles (Figure 4) and Cu precursor exposure time/dose (Figure 5). Figure 4a shows that, for 50 cycles, nominal growth rates of Cu and Cu₃N on SiO₂ wafers are ~1.8 and 0.2 Å/cycle, respectively. These values are consistent with previous reports by Li et al.^{16,17} It is also seen from Figures 4a and 5a that, for <25 cycles, the Cu thickness on SiO₂ wafers is in most cases close to our detection limit (~0.2 Å), is poorly reproducible, and, within such a large scatter in experimental data points, appears to be independent of the number of cycles or exposure time to

(12) Gordon, R. G.; Hausmann, D.; Kim, E.; Shepard, J. *Chem. Vap. Deposition* **2003**, *9*, 73.

(13) Elam, J. W.; Routkevitch, D.; Mardilovich, P. P.; George, S. M. *Chem. Mater.* **2003**, *15*, 3507.

(14) In the figure captions and in the text, t_{CuAMD} is the time of exposure to the [Cu(^{*t*}Bu-Me-amd)]₂ precursor (the first half-cycle); $t_{\text{H}_2/\text{NH}_3}$ is the exposure time to either H₂ (for Cu metal depositions) or NH₃ (for Cu₃N depositions) precursors (the second half-cycle); t_{pur1} and t_{pur2} are N₂ purge times after exposure to precursors in the first and second half-cycles, respectively; and N_{cyc} is the number of cycles.

(15) Note that the average diameter of Cu nanoparticles (25 nm) is slightly larger than the BJH average pore diameter (18 nm) of 25 mg cm⁻³ AGs. This apparent inconsistency could be reconciled by noting that the size distributions of both Cu nanoparticles and pores are broad, with BJH pore diameters extending to over 100 nm.

(16) Li, Z.; Rahtu, A.; Gordon, R. G. *J. Electrochem. Soc.* **2006**, *153*, C787.

(17) Li, Z.; Gordon, R. G. *Chem. Vap. Deposition* **2006**, *12*, 435.

(18) See, for example, Satoh, S.; Matsuyama, I.; Susa, K. *J. Non-Cryst. Solids* **1995**, *190*, 206. Reichenauer, G.; Stumpf, C.; Fricke, J. *J. Non-Cryst. Solids* **1995**, *186*, 334.

(19) Such a maximum Cu concentration was close to the monolith surface, and the depth profiles of Cu for all the samples exposed to both half-cycles were qualitatively similar to those shown in the inset of Figure 3.

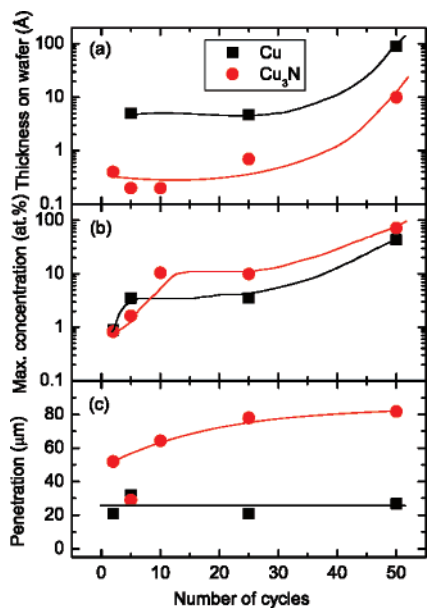


Figure 4. Dependencies of (a) Cu thickness on SiO₂ wafers, (b) the maximum Cu concentration in AGs, and (c) Cu penetration depth on the number of ALD cycles for both Cu (squares) and Cu₃N (circles) depositions. ALD parameters: $t_{\text{CuAMD}} = t_{\text{H}_2/\text{NH}_3} = 150$ s, $t_{\text{pur1}} = t_{\text{pur2}} = 30$ s. All AG monoliths had an initial density of 25 mg cm⁻³. Solid lines are to guide the reader's eye.

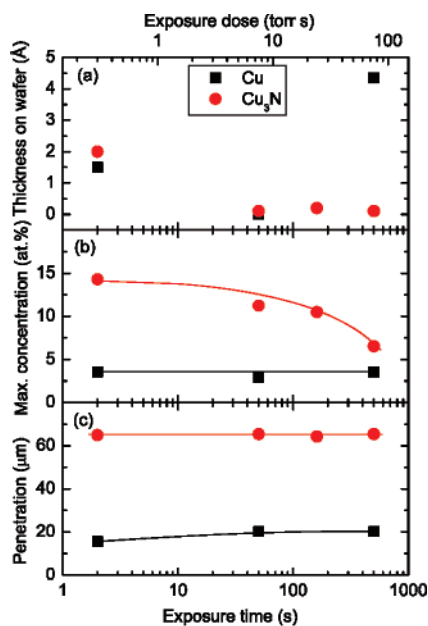


Figure 5. Dependencies of (a) Cu thickness of SiO₂ wafers, (b) the maximum Cu concentration in AGs, and (c) Cu penetration depth on the exposure time to the Cu precursor for both Cu (squares) and Cu₃N (circles) depositions. ALD parameters: $N_{\text{cyc}} = 10$, $t_{\text{pur1}} = t_{\text{pur2}} = 30$ s, $t_{\text{H}_2/\text{NH}_3} = 150$ s. All AG monoliths had an initial density of 25 mg cm⁻³. Solid lines are to guide the reader's eye. Note that, in panel a, the Cu thickness on SiO₂ wafers is poorly reproducible and, in most cases, close to the detection limit of ~ 0.2 Å.

the Cu precursor for both Cu and Cu₃N processes. This is consistent with the paucity of nucleation sites (presumably, Si–OH groups¹⁶) on the SiO₂ surface, accounting for the very small amounts of Cu deposited on nominally flat substrates for <25 cycles. This difficulty with nucleation on SiO₂ could possibly be alleviated by growing Cu on Al₂O₃ instead of on SiO₂.¹⁶ For example, a nucleation layer of Al₂O₃ has been used in previous ALD studies of ZnO, W, and Ru on AGs.^{2–5} However, additional

systematic studies of the area density of the nanoparticles deposited in the regime of a small number of cycles are currently needed to better understand the effects of surface chemistry and topography as well as the deposition parameters on the ALD nucleation of Cu and Cu₃N.

The dependence of the maximum Cu concentration in AG monoliths on the number of cycles, illustrated in Figure 4b, shows that, for ≥ 10 cycles, more Cu is deposited on AG ligaments in the Cu₃N than in the Cu ALD process. Within experimental error, the penetration depth is independent of the number of cycles for Cu [Figure 4c]. This constancy makes sense in a diffusion picture if the surface with which Cu precursor molecules are colliding remains the same during these cycles. Because the deposited Cu agglomerates [see Figure 2a], most of the AG surface remains as silica during the relatively small number of cycles used in this study (≤ 50). In contrast, Cu₃N appears to agglomerate slightly less than Cu [Figure 2b], resulting in a better coverage of the silica surface with Cu₃N during the first few cycles. Evidently, the diffusion of Cu precursor molecules colliding against a silica surface is somewhat slower than their diffusion over a Cu₃N surface. Such differences in the diffusion rate could arise if Cu precursor molecules have “sticky” collisions with a larger residence time on silica than on Cu₃N; we discuss this effect in more detail below.

Additional differences between Cu and Cu₃N ALD processes are revealed by Figure 4c, showing that the ALD of Cu₃N results in ~ 3 times deeper penetration of coating than the ALD of Cu metal. This difference between the two materials could be explained by the Knudsen diffusion model, which predicts that the penetration depth scales inversely as the square root of the saturation coverage of Cu atoms on a flat surface.¹² From Figure 4a, the saturation coverage of Cu is ~ 10 times that of Cu₃N. Hence, the penetration of Cu₃N should be larger than that of Cu by a factor of $\sim \sqrt{10} \approx 3$, in agreement with the results in Figure 4c. This large difference between the coating penetration depths for Cu and Cu₃N depositions indicates the importance of the surface chemistry.

We can also use the Knudsen diffusion model to try to predict the actual values of the penetration depths, in addition to their relative values discussed above. According to the Knudsen diffusion model,¹² the penetration depth of ALD coating into a straight hole depends on the saturation ALD thickness, the precursor partial pressure and exposure time, the precursor molecular mass, and the temperature. Of course, in an AG, the hole is not straight, so we assume that the tortuous diffusion path is twice as long as a straight line perpendicular to the surface of an AG monolith. Using the saturated ALD surface coverage for Cu (0.92 Å per cycle¹⁶) and Cu₃N (0.3 Å per cycle¹⁷), a precursor partial pressure of 0.12 Torr, an exposure time of 600 s, a molecular mass of 465.67 amu, and a temperature of 190 °C, we calculated the penetration depths and coated aspect ratios listed in Table 2. The simple theory is in good agreement with the experimental penetration depths for the pressure used in all our experiments (0.12 Torr, line 1 in Table 2). The following lines of Table 2 give the predicted penetration depths and coated aspect ratios for higher partial pressures. If the precursor partial pressure were raised to 120 Torr (which is the extrapolated vapor pressure at a bubbler temperature of 190 °C), the penetration depths are predicted to rise to around a millimeter. At a bubbler temperature of 190 °C, the precursor in the liquid-phase decomposes with a half-life of ~ 1 month,¹¹ so it would be impractical to use bubbler temperatures above this temperature. Also, the substrate temperature would need to be increased to prevent multilayer adsorption on the AGs. Flash vaporization of

Table 2. Depth of Penetration of Cu and Cu₃N into AGs^a

pressure (Torr)	Cu depth (mm)		Cu aspect ratio		Cu ₃ N depth (mm)		Cu ₃ N aspect ratio	
	obs.	calc.	obs.	calc.	obs.	calc.	obs.	calc.
0.12	0.025	0.025	2.8×10^3	2.7×10^3	0.08	0.06	8.9×10^3	6.8×10^3
1.2	n/a	0.08	n/a	8.5×10^3	n/a	0.21	n/a	2.4×10^4
12	n/a	0.25	n/a	2.7×10^4	n/a	0.60	n/a	6.8×10^4
120	n/a	0.75	n/a	8.5×10^4	n/a	2.1	n/a	2.4×10^5
1200	n/a	2.4	n/a	2.7×10^5	n/a	6.0	n/a	6.8×10^5
12000	n/a	7.5	n/a	8.5×10^5	n/a	21	n/a	2.4×10^6

^a The 0.12 Torr line gives the observed penetration depths. The values in the lines below are predictions based on scaling by the square root of the precursor partial pressure (see text for more details). The experimental aspect ratios are the penetration depth times 2 (to account roughly for the tortuous diffusion path in the AG being longer than a straight line) divided by an average pore diameter of 18 nm.

the precursor could be used to obtain vapor concentrations higher than 120 Torr, but vaporization and substrate temperatures need to be kept below ~ 250 °C to avoid decomposition of the precursor. In this way, the Knudsen diffusion model predicts that it may be possible to extend the penetration depths to the centimeter range.

Further insight into the deposition mechanism is provided by studying the process dependence on the exposure time to the Cu precursor (or Cu precursor exposure dose, which is a product of exposure time and precursor vapor pressure). It is seen from Figure 5b that the maximum Cu concentration is independent of the exposure time for Cu and rapidly decreases with exposure time for Cu₃N deposition. This decrease suggests that the surface reactions forming Cu₃N may be partly reversible, rather than irreversible, as is usually assumed. Finally, Figure 5c shows that the Cu penetration depth very slightly increases for Cu and is almost independent of the exposure time for Cu₃N.

Results from Figures 2–5 demonstrate that both Cu and Cu₃N depositions on AGs are far from being “ideal” ALD processes and cannot be explained completely by Knudsen diffusion of the heavier precursor molecules, as typically assumed.^{2–7,12,13} Indeed, in such an ideal case, the ALD proceeds as a self-limiting reaction when, in the first half-cycle, Cu precursor molecules diffuse into the pores, decorating the ligament surfaces by only one monolayer of *chemisorbed* molecules. These chemisorbed precursor molecules have infinite surface residence time, and no multilayer adsorption takes place. The precursor penetration depth is diffusion-limited and, hence, scales as a square root of the precursor exposure time. During the first N₂ purge following the exposure to the Cu precursor, the unused precursor molecules and any possible byproducts of precursor chemisorption diffuse out of the pores. During the second half-cycle of such an ideal ALD scenario, the porous monolith is exposed to H₂ or NH₃ molecules, which diffuse into the pores and experience a chemical reaction with the Cu-containing molecules chemisorbed onto the ligament surfaces during the first half-cycle. The second purge carries away all the presumably highly volatile reaction byproducts and the unused precursor molecules. These processes are repeated in all subsequent cycles.

In the ideal ALD process described above, (i) coating is conformal, (ii) the Cu thickness on wafers²⁰ linearly depends on the number of cycles, and (iii) the penetration depth of coating into the monolith is independent of the number of cycles. In addition, the Cu precursor exposure time should not affect the Cu film thickness on wafers and the maximum Cu concentration in AGs (for exposures sufficient for the formation of a monolayer of chemisorbed precursor molecules), while the penetration depth

of coating should increase as a square root of the exposure time, as mentioned above.

Therefore, data from Figures 2–5 indicate a highly nonideal ALD behavior, suggesting that the deposition is controlled not only by the idealized Knudsen diffusion of heavier precursor molecules but also by some other processes. Below, we discuss some possible mechanisms of such a nonideal ALD behavior.

We first note that the limited deposition depth of Cu in AG monoliths, experimentally observed here, cannot be attributed to possible plugging of the pores with Cu or Cu₃N nanoparticles, blocking the diffusion path of precursor molecules. Such a pore plugging scenario is not consistent with the following experimental observations: (i) the dependence on the number of cycles shown in Figure 4c is not characteristic of pore plugging; (ii) Cu depth profiles similar to those illustrated in Figure 3 have been observed for only two cycles, when pore plugging is highly unlikely; (iii) the depth profiles of Cu do not reveal any surface spikes, in contrast to what would be expected if pore plugging occurred; and (iv) our ALD experiments with other metals, including Ru,⁵ Pt,⁶ and Fe,⁷ with highly variable tendency to agglomerate into nanoparticles during deposition, have revealed qualitatively similar depth profiles of coatings.

In addition to the mechanisms assumed in the idealized ALD scenario discussed above, deposition onto substrates with ultrahigh aspect ratios is affected by intricate processes of the adsorption–desorption equilibrium of precursor and reaction product molecules. These include (i) multilayer adsorption of the precursor molecules, (ii) reversibility of precursor chemisorption reactions for long exposures, and (iii) contamination of ligament surfaces with reaction byproducts. In particular, diffusion of Cu precursor and reaction product molecules is likely to be a very slow process because of the highly tortuous morphology of AGs as well as large masses and, more importantly, reactivity of precursors and reaction byproducts. It has been shown that the reaction of H₂ or NH₃ gas with liquid [Cu(^tBu-Me-amd)]₂ at 120 °C gives *N,N'*-di-*sec*-butylacetamide as the reaction product (Figure 1b),^{16,17} which are reactive (sticking) molecules, mainly because of the interaction of the amino groups with the Cu or Cu₃N surface.²¹ Since the number of gas–pore wall collisions scales with the square of the aspect ratio,²² even a relatively small residence time of physisorption (e.g., a few microseconds) would dramatically reduce gas diffusion through nanoporous solids with ultrahigh aspect ratios of $\geq 10^3$ compared to the case of the ideal ALD process with zero residence time for multilayer adsorption.

(21) It is interesting to note that, if such contamination by reaction products is the major process limiting the depth of Cu and Cu₃N coatings in nanoporous monoliths, it must occur even during the very first cycle. Indeed, depth profiles of Cu for only two ALD cycles of either Cu or Cu₃N are qualitatively similar to those for depositions involving a larger number of cycles (Figure 4).

(22) Horton, W. S. *J. Phys. Chem.* **1964**, *68*, 2278.

(20) Note that the atomic concentration of Cu in ligaments, shown in Figures 3–5, should be directly proportional to the Cu thickness on wafers for film thicknesses significantly smaller than the ligament and pore diameters.

This mechanism, however, also predicts a stronger increase of penetration depth with exposure than is seen experimentally.

Moreover, we cannot completely rule out some physisorption and dissociation of the second half-cycle precursors (i.e., H₂ and NH₃) on the surface of SiO₂ AG ligaments coated with Cu or Cu₃N nanoparticles.²³ We, however, argue that the nonideal ALD behavior observed here is predominantly related to processes occurring during the first half-cycle, involving the diffusion and interaction of Cu precursor molecules and their reaction byproducts. This argument is based on the following facts: (i) [Cu(^tBu-Me-amd)]₂ molecules are much larger, heavier, and more reactive than either H₂ or NH₃; (ii) the vapor pressure during the second half-cycle was much larger; and (iii) NH₃ should interact much stronger than H₂ with pore walls and, hence, result in a shallower penetration of Cu coating, which contradicts our observations.

We also note that the limited penetration depth of Cu coating revealed in Figures 4 and 5 is not related to a relatively short purge time of 30 s used in this set of experiments. Indeed, Figure 3 shows that a much larger purge time of 1500 s does not improve the coating penetration depth. Our additional experiments have shown that changing the purge time from 5 to 100 s (with $N_{\text{cyc}} = 10$, $t_{\text{CuAMD}} = t_{\text{H}_2/\text{NH}_3} = 50$ s, and $t_{\text{pur1}} = t_{\text{pur2}}$)¹⁴ does not improve the Cu penetration depth. Purge times long enough for unused precursor molecules and reaction byproducts to diffuse out of the nanoporous network are, nevertheless, critical for achieving an ideal ALD behavior,⁸ and this process parameter deserves additional studies.

Some of the features of the Cu depth profiles experimentally observed (see Figure 3) could also be explained by a possible decomposition of Cu precursor molecules after multiple collisions with ligament surfaces. Note that, because of the tortuous morphology of nanoporous substrates, even for very small thermal accommodation coefficients,²⁴ precursor molecules quickly reach thermal equilibrium with the substrate, resulting in higher translational, rotational, and vibrational energies, which could aid precursor decomposition. Moreover, the fact that the precursor is stable at the deposition temperature in the liquid phase¹¹ does not necessarily indicate that it will be stable inside the pores during collisions with (or diffusion on) the ligament surfaces. Particularly, the presence of metal nanoparticles (see Figure 2) could have a catalytic effect on the decomposition process.

Such a scenario involving precursor decomposition in AG pores appears to be supported by our experiment with the following ALD parameters:¹⁴ $N_{\text{cyc}} = 10$, $t_{\text{CuAMD}} = 50$ s, $t_{\text{pur1}} = 89$ s, $t_{\text{H}_2/\text{NH}_3} = 0$ s, and $t_{\text{pur2}} = 0$ s (i.e., exposures to only the first half of each cycle). Without precursor decomposition, for such conditions, Cu deposition should be limited to one chemisorbed monolayer of the precursor molecules. The Cu thickness on SiO₂ wafers was indeed close to the detection limit of our RBS experiment (~ 0.2 Å), while the amount of Cu deposited on the inner surfaces of an AG at depths of ≥ 15 μm was substantial, with a maximum Cu concentration of 3.2 atom % and a Cu penetration depth of 43 μm. This is comparable to Cu concentrations for conditions when samples were exposed to both half-cycles (see Figures 4 and 5), suggesting that some precursor decomposition occurs within pores during Cu deposition. However, thermal decomposition cannot play a dominant role

in the case of Cu₃N because a much larger amount of Cu₃N is deposited in the presence of NH₃ than in such a control experiment without NH₃. Further direct experimental studies of the chemical state of chemisorbed precursor molecules (information not provided by RBS) are currently needed to better understand the thermal stability of the precursor within pores.

Although additional studies are currently needed to ascertain the relative contributions of the processes discussed above, our data suggest that most of the advanced precursors developed for ALD on substrates with moderate aspect ratios have limited suitability for uniform coating nanoporous monoliths over millimeter penetration depths. The calculations in Table 2 illustrate the very high vapor pressures needed even if the ALD properties of the precursors were ideal. All of the nonideal mechanisms that we have suggested would tend to reduce the achievable penetration depth below these ideal values. Indeed, the novel ALD precursors that have received the most attention for the past decade (including the precursors used in the present study) are heavy and bulky molecules whose reaction byproducts often involve complex hydrocarbons with relatively low volatility.⁸ Coating substrates with ultrahigh aspect ratios require process parameters ensuring that precursors are highly volatile, stable against decomposition *inside the pores* for the periods of time required for precursor exposure and purging, and generate highly volatile and stable reaction products.

In conclusion, we have studied the deposition of metallic Cu and semiconducting Cu₃N nanoparticles on the inner surfaces of nanoporous silica AG monoliths with ultrahigh aspect ratios of $\sim 10^5$. Our results have demonstrated that, for both Cu and Cu₃N, the deposition behavior on the inner surfaces of nanoporous solids can differ from that for substrates with smaller aspect ratios ($\lesssim 10^3$) and is more complex than previously believed. The ALD process appears to be influenced by precursor reactivity and adsorption–desorption equilibrium processes of precursor and reaction product molecules, and not only by the Knudsen diffusion of precursor molecules, as believed previously. We suggest that uniform coating of macroscopic nanoporous monoliths requires a development of a new class of precursors and process parameters specifically geared for coating ultrahigh aspect ratio solids. Such precursors must be extremely volatile, very stable against thermal decomposition, and have reaction byproducts that are sufficiently volatile to be effectively removed from the pores with a highly tortuous morphology, inherent to most nanoporous solids.

Experimental Section

Amorphous silica AGs were synthesized as described in detail in ref 25. Bulk densities of AGs were determined by measuring the dimensions and mass of monolithic samples. Surface area determination and pore volume analysis, summarized in Table 1, were performed by Brunauer–Emmett–Teller (BET) and Barrett–Joyner–Halenda (BJH) methods using an ASAP 2000 Surface Area Analyzer (Micromeritics Instrument Corp.), as described elsewhere.²⁵

The ALD was performed in a viscous flow reactor described previously.^{16,17} Several-millimeters-thick monolithic silica AGs with initial densities in the range of 10–50 mg cm⁻³, glued to Si wafers, were coated with either metallic Cu or semiconducting Cu₃N by alternating exposures to the following precursors: (i) a mixture of [Cu(^tBu-Me-amd)]₂ and N₂ and (ii) H₂ (for Cu) or NH₃ (for Cu₃N). The total system pressure during precursor exposures was kept at ~ 5 and ~ 40 Torr for [Cu(^tBu-Me-amd)]₂ and H₂/NH₃, respectively. Temperatures of the liquid Cu precursor and AG substrates were

(23) See, for example, Morrow, B. A.; Cody, I. A.; Lee, L. S. M. *J. Phys. Chem.* **1976**, *80*, 2761. Fubini, B.; Bolis, V.; Cavenago, A.; Garrone, E.; Ugliengo, P. *Langmuir* **1993**, *9*, 2712. Sandoval, M. J.; Bell, A. T. *J. Catal.* **1993**, *144*, 227. Neurock, M.; van Santen, R. A.; Biemolt, W.; Jansen, A. P. *J. Am. Chem. Soc.* **1994**, *116*, 6860.

(24) Saxena, S. C.; Joshi, R. K. *Thermal Accommodation Coefficient and Adsorption of Gases*; McGraw-Hill: New York, 1979.

(25) Hrubesh, L. W.; Tillotson, T. M.; Poco, J. F. In *Chemical Processing of Advanced Materials*; Hench, L. L., West, J. K., Eds.; Wiley: New York, 1992; p 19.

kept in the ranges of ~ 110 – 120 °C and ~ 185 – 190 °C, respectively. The vapor pressure of $[\text{Cu}(\text{}^i\text{Bu-Me-amd})]_2$ over the liquid phase is ~ 1 Torr at 120 °C, corresponding to a Cu precursor vapor pressure of ~ 0.12 Torr in the deposition chamber during exposures. Between each exposure, the reactor was first purged with ultrahigh purity N_2 (with the system at ~ 0.3 Torr) and then evacuated below 50 mTorr. Prior to deposition, all AGs were held at ~ 185 °C under a N_2 flow at ~ 0.3 Torr for 3 h to remove adsorbates. Silicon wafers with thermally grown ~ 100 – 300 -nm-thick surface oxide layers were used as control samples during each ALD run on AGs.

In $[\text{Cu}(\text{}^i\text{Bu-Me-amd})]_2$ molecules (Figure 1a), each Cu atom is bound to two amidinate ligands, which makes the molecule stable, with a half-life time of 33 days at 190 °C (the deposition temperature used in this study) in a liquid phase.¹¹ Additional details about precursor synthesis, properties, and its suitability for ALD of Cu and Cu_3N on substrates with moderate aspect ratios of $\lesssim 40$ can be found in refs 11, 16, and 17.

Depth uniformity of Cu coating in AG monoliths was studied by RBS spectrometry with 2 MeV ${}^4\text{He}^+$ ions incident at the normal to

the sample surface and backscattered into a detector at 164° relative to the incident beam direction. To extract the depth profiles of the Cu atomic concentration from RBS spectra, we used the RUMP code.²⁶ In all RUMP simulations, the composition of AG ligaments was assumed to be SiO_2Cu_x ; i.e., light impurities such as H, C, O, and N, whose concentrations are very challenging to estimate from RBS data, were not taken into account. This assumption does not affect the conclusions of this work, which primarily concerns the depth uniformity of ALD on nanoporous monoliths. Finally, the AG microstructure was studied by bright-field transmission electron microscopy in a Philips CM300FEG transmission electron microscope operated at 300 kV.

Acknowledgment. Work at LLNL was performed under the auspices of the U.S. DOE by the University of California, LLNL, under Contract No. W-7405-Eng-48.

LA7018617

(26) Doolittle, L. R. *Nucl. Instrum. Methods B* **1985**, *9*, 34.